Solar Energy Materials & Solar Cells 94 (2010) 1704–1710

Contents lists available at ScienceDirect

Solar Energy Materials & Solar Cells

journal homepage: www.elsevier.com/locate/solmat

Evaluation of thermal radiation dependent performance of GaSb thermophotovoltaic cell based on an analytical absorption coefficient model

Y. Wang [a,*], N.F. Chen [b,*], X.W. Zhang [a], T.M. Huang [a], Z.G. Yin [a], Y.S. Wang [a], H. Zhang [a]

[a] Key Laboratory of Semiconductor Materials Science, Institute of Semiconductor, Chinese Academy of Sciences, Beijing 100083, China
[b] School of Renewable Energy Engineering, North China Electric Power University, Beijing 102206, China

ARTICLE INFO

Article history:
Received 10 September 2009
Accepted 10 May 2010

Keywords:
Thermophotovoltaic
Gallium antimonide
Absorption coefficient

ABSTRACT

Applying the model dielectric function method, we have expressed the absorption coefficient of GaSb analytically at room temperature relating to the contribution of various critical points of its electronic band structure. The calculated absorption spectrum shows good agreement with the reported experimental data obtained by spectral ellipsometry on nominally undoped sample. Based on this analytical absorption spectrum, we have qualitatively evaluated the response of active absorbing layer structure and its photoelectric conversion properties of GaSb thermophotovoltaic device on the perturbation of external thermal radiation induced by the varying radiator temperature or emissivity. Our calculation has demonstrated that desirable thickness to achieve the maximum conversion efficiency should be decreased with the increment of radiator temperature and the performance degradation brought by any structure deviation from its optimal one would be stronger meanwhile. For the popular radiator temperature, no more than 1500 K in a real solar thermophotovoltaic system, and typical doping profile in GaSb cell, a reasonable absorbing layer structure parameter should be controlled within 100–300 nm for the emitter while 3000–5000 nm for the base.

1. Introduction

In recent years, there is a renewed interest in solar thermophotovoltaic (STPV) [1] because of considerable progress received in the fabrication of high-quality, low-bandgap semiconductor converters, e.g., gallium antimonide (GaSb) as well as its ternary or quaternary alloys [2–5]. When compared with conventional photovoltaic (PV) application, an intermediate emitter, generally made by refractory materials such as tungsten [6] or ceramic oxides [7], is particularly introduced in thermophotovoltaic (TPV) scheme to heat itself by absorbing the concentrated solar illumination, then low-bandgap converters are used to convert the reemitted thermal irradiation of heated emitter into electric energy. Due to close space distance between emitter and converters, high density electric output and the generation of heat simultaneously are promised. Moreover, by modulating the thermal irradiation through some artificial engineering [8], a competitive thermal-to-electric conversion efficiency (η) is also attainable because of the enhanced spectral match between the incident spectrum and response of TPV cell, showing the potential application in both terrestrial and space [1,9].

However, for the real outdoor STPV application, operating temperature of intermediate emitter in a real STPV prototype is very difficult to keep invariant because the incident intensity of solar illumination is different from time to time, leading to the marked variation of thermal irradiation and further resulting in the potential perturbation on the generation of electricity and output stability. It is therefore very necessary to reveal this perturbation on device performance comprehensively. Disappointingly, even for the dominant GaSb device, relatively little work has been done to perform the design and structure optimization of GaSb cell because of the insufficient knowledge of device related parameters [10,11]. For example, both Stollwerck et al. [10] and Martín and Algora [11] have made an attempt to quantify the optical absorption in device simulation, but no analytical expression was given explicitly there. Therefore, the underlying goal of this work is to establish an analytical model for the absorption spectrum of GaSb in the range 0.5–6 eV, and further to enhance the qualitative understanding of performance perturbation of GaSb TPV cell illuminated by a varying incident radiation for the aforementioned reason.

This paper is organized as follows. In Section 2 we briefly describe the combined theoretical method to analytically express the absorption coefficient of GaSb, and the detailed procedure to simulate the performance of GaSb cell is presented in Section 3. The calculated result and comprehensive discussion is given in Section 4, and in Section 5 we conclude with a summary.

* Corresponding author. Tel.: +86 10 82304458; fax: +86 10 82304588.
E-mail addresses: ywang@semi.ac.cn (Y. Wang), nfchen@ncepu.edu.cn (N.F. Chen).

0927-0248/$ - see front matter © 2010 Elsevier B.V. All rights reserved.
doi:10.1016/j.solmat.2010.05.032

2. Analytical model for GaSb absorption coefficient

With an attempt to perform the structure optimization of GaSb cell, an accurate knowledge of optical absorption $\alpha(E)$ related to the radiation energy E of incident photon is thus strongly desirable. However, in spite of its significance in STPV application, relatively little investigation has been reported to determine $\alpha(E)$of GaSb. Experimentally, using spectral ellipsometry (SE) measurements, both Ferrini et al. [12] and Aspnes and Studna [13] have measured the room temperature complex dielectric function $\varepsilon(E)[=\varepsilon_1(E)+i\varepsilon_2(E)]$ of GaSb on nominally undoped sample, and the derived $\alpha(E)$ has been given as we depicted schematically in Fig. 1 with different symbols, circle for the former while star for the latter. Disappointedly, a desirable analytical form of $\alpha(E)$, important and convenient for the device simulation, was not given explicitly there. In the theoretical aspect, in the framework of the simple band-to-band single particle transition, Adachi [14] proposed a model dielectric function (MDF) method to calculate the optical absorption of zinc-blende-type semiconductor analytically in terms of its electronic band structure. Although a satisfied fit between theoretical calculation and scattered experimental data was not obtained, the underlying principle of this proposal, decomposing the integrated absorption of material under consideration into the specific contribution of various type critical points (CP) in its Brillouin Zone (BZ), are involved into subsequent model calculations [15–19].

Specifically, in zinc-blende-type GaSb, spin–orbit interaction splits $\Gamma^v_{15}(\Gamma^c_{15})$valence (conduction) band into $\Gamma^v_7(\Gamma^c_7)$ (degenerate band) and $\Gamma^v_8(\Gamma^c_8)$ (spin-split off band) with an energy splitting $\Delta_0(\Delta'_0)$, also the L^v_3 valence band is split into $L^v_{4,5}$and L^v_6 by spin–orbit interaction with an energy splitting Δ_1 [20]. Thus, the important CPs in BZ can be labeled as direct gap $E_0[\Gamma^v_8\rightarrow\Gamma^c_6]$, spin split off component $E_0+\Delta_0[\Gamma^v_7\rightarrow\Gamma^c_6]$, spin–orbit split doublet $(E_1[L^v_{4,5}\rightarrow L^c_6]$, $E_1+\Delta_1[L^v_6\rightarrow L^c_6])$, indirect gap E^{ID}_g $(E_X[\Gamma^v_8\rightarrow X^c_6]$ or $E_L[\Gamma^v_8\rightarrow L^c_6])$ and higher-lying E_2 transition along $\langle 1\,1\,0\rangle$ or near X point. Based on these CPs and additional higher CP if necessary, several modified MDF methods [16–19] have been proposed to express $\alpha(E)$ of GaSb analytically, but the detailed comparison between experimental data and theoretical calculation, to our knowledge, is still absent from the literature.

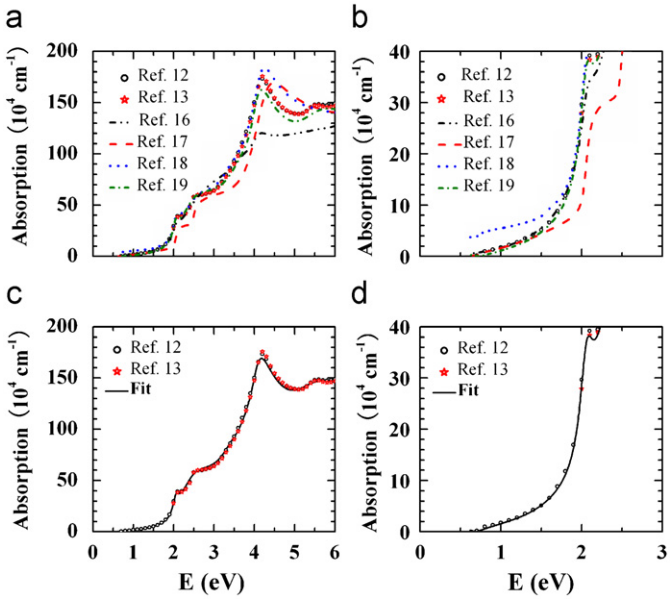

Fig. 1. Comparison of theoretical calculation and experimental measurements on GaSb absorption coefficient: (a) several reproduced theoretical curves calculated from the proposed physical models are compared with the experimental data measured by Ferrini et al. (open circle symbol) and Aspnes et al. (star symbol), and for clarity an expanded version in the range 0–3 eV is schematically shown in (b). Our calculated curves based on an improved model is shown and compared with experiments in (c), and in (d) the expanded picture near the fundamental energy is displayed.

In the top panel of Fig. 1, the reproduced theoretical curves calculated from the suggested parameters for each proposed model are shown for comparison, and for clarity, in Fig. 1(b), an expanded version near band edge is also shown. Evidently, both the calculation of Gonzalez-Cuevas et al. [17] (dashed line) and Djurišić et al. [16] (dash-dot-dot line) by developing the Adachi's modified MDF method [15], are failure to fit the experimental data well, indicating the theoretical insufficient of band-to-band single particle transition. However, it is noteworthy that additional incorporation of a frequency-dependent broadening [21–23] in Ref. [16] can give significant improvement in the range 0.5–2 eV while for E larger than 3 eV the increasing discrepancy are observed. In order to clarify the CPs in $\alpha(E)$ of GaSb, Muñoz et al. [18] have performed SE measurements again on nominally undoped sample and tabulated the model parameters by fitting their experimental data with the Holden's MDF [24,25] theory, where the contribution associating with the discrete and continuous exciton effect is also included. Unfortunately, direct comparison of $\alpha(E)$ between their experiment and theoretical calculation was absent from their report. For the comparison, we have reproduced their theoretical curve (short dashed line in Fig. 1) in line with their preferential model and suggested parameters. It is easily seen that, with the exception of optical absorption near the band edge (see Fig. 1(b)) and beyond the E_2 points (4.1 eV), excellent fit can be attained. To overcome the overestimation of theoretical $\alpha(E)$ near band edge, Djurišić et al. [19] have received significant improvement (see dash-dot line in Fig. 1) by replacing the Lorentzian broadening with an adjusting broadening. However, there is an unexpected degradation of optical absorption in the range $2.54(E_1+\Delta_1)$–$4.1(E_2)$ eV.

Based on the above analysis, we have improved the physical model to express GaSb optical absorption analytically by inheriting good feature from the aforementioned models. In the down panel of Fig. 1, our calculated result is shown for the comparison. Obviously, the impressive fit between our calculation and reported experimental data cannot only be attained near the band edge, but also for the whole interested range. In the following, specific model we used are briefly summarized and the corresponding parameter are tabulated in Table 1.

In our calculation, the modified Holden's MDF model [19] is mainly employed and the involved CPs are E_0, $E_0+\Delta_0$, E_1, $E_1+\Delta_1$, E_2, $E'_0[\Gamma^v_8\rightarrow\Gamma^c_7]$, $E'_0+\Delta'_0[\Gamma^v_8\rightarrow\Gamma^c_8]$, and an unlabeled CP E_3 to improve the fit for the broadening peak located at $E=5.3$ eV or so. Moreover, any contribution from the indirect transition is not included in our simulation. Following the modified Holden's MDF

Table 1
Values of model parameters to calculate the absorption spectrum of GaSb.

Parameters	Value	Parameters	Value	Parameters	Value
E_0 (eV)	0.728	E_1 (eV)	2.189	E'_0 (eV)	3.400
A (eV^2)	0.096	C (eV^2)	6.696	$F(E'_0)$ (eV^2)	13.879
$\Gamma_0=\Gamma^{ex}_0$(eV)	0.084	Γ_1 (eV)	0.101	$\Gamma(E'_0)$ (eV)	0.782
α_0	0.039	α_1	0.001	$E'_0+\Delta'_0$ (eV)	3.790
R_0 (eV)	0.0016	R_1 (eV)	0.035	$F(E'_0+\Delta'_0)$(eV^2)	14.795
$E_0+\Delta_0$ (eV)	1.453	$E_1+\Delta_1$ (eV)	2.544	$\Gamma(E'_0+\Delta'_0)$(eV)	0.644
B (eV^2)	0.037	D (eV^2)	34.708	E_2 (eV)	4.050
$\Gamma_{s0}=\Gamma^{ex}_{s0}$ (eV)	0.180	Γ_{1s}(eV)	0.359	$F(E_2)$ (eV^2)	24.484
α_{s0}	0.039	α_{1s}	0.001	$\Gamma(E_2)$ (eV)	0.481
R_{s0} (eV)	0.0016	R_{1s}	0.035	E_3 (eV)	5.310
ε_∞	0.775	$F(E_3)$ (eV^2)	19.771	$\Gamma(E_3)$ (eV)	1.379

method, taking into account the discrete and continuous exciton contribution together, the complex dielectric function $\varepsilon(E)$ responsible for the CP E_0 can be written as [19]

$$\varepsilon^{\mathrm{I}}(E)=\frac{A}{2}\sum_{n=1}^{\infty}\frac{4R_0}{n^3E_{ex,n}^2}\left(\frac{1}{E+E_{ex,n}+i\Gamma_n}-\frac{1}{E-E_{ex,n}+i\Gamma_n}\right)-\frac{A}{2}\left[S(\xi(E+i\Gamma_0))+S(\xi(-E-i\Gamma_0))\right]+\frac{A}{2(E+i\Gamma_0)^2}\left[g(\xi(E+i\Gamma_0))+g(\xi(-E-i\Gamma_0))-2g(\xi(0))\right] \tag{1}$$

where

$$\xi^2(z)=E_0-z/R_0 \tag{2}$$

$$S(\xi)=\sum_{n=1}^{\infty}\frac{2}{n^3E_{ex,n}^2}\frac{1}{\xi^2-1/n^2} \tag{3}$$

$$g(\xi)=-\pi\cot\left[\frac{\pi}{\xi}\right]-\ln(\xi^2) \tag{4}$$

where A is the strength parameter, R_0 is the effective Rydberg energy, E_0 is the energy for the considered CP, Γ_0 is the broadening constant for band-to-band contributions, while $\Gamma_n[=\Gamma_0-(\Gamma_0-\Gamma_{ex,1})/n^2]$ is the broadening factor for discrete excitons with $\Gamma_{ex,1}$denoting the broadening constant of the ground state exciton, and $E_{ex,n}[=E_0-R_0/n^2]$ is the energy of exciton level. Moreover, with the replacement of strength $A\rightarrow B$, CP's energy $E_0\rightarrow E_0+\Delta_0$, and broadening constant $\Gamma_{0s}\rightarrow\Gamma_0$, the same expression would be obtained for the $E_0+\Delta_0$ transition.

For the 2D-M_0-type CP E_1, the corresponding $\varepsilon(E)$ can be modeled by the below equation [19]

$$\varepsilon^{\mathrm{II}}(E)=\frac{C}{2}\sum_{m=1}^{\infty}\frac{32R_1}{(2m-1)^3E_{ex,m}^2}\left(\frac{1}{E+E_{ex,m}+i\Gamma_1}-\frac{1}{E-E_{ex,m}+i\Gamma_1}\right)-\frac{C}{2}\left[S_1(\xi(E+i\Gamma_1))+S_1(\xi(-E-i\Gamma_1))\right]+\frac{C}{2(E+i\Gamma_1)^2}\left[g_1(\xi(E+i\Gamma_1))+g_1(\xi(-E-i\Gamma_1))-2g_1(\xi_{(0)})\right] \tag{5}$$

where

$$E_{ex,m}^2=\frac{E_1-4R_1}{(2m-1)^2} \tag{6}$$

$$S_1(\xi)=\sum_{m=1}^{\infty}\frac{16}{(2m-1)^3E_{ex,m}^2}\frac{1}{\xi^2-4/(2m-1)^2} \tag{7}$$

$$g_1(\xi)=\pi\tan\left[\frac{\pi}{\xi}\right]-\ln(\xi^2) \tag{8}$$

$$\xi^2(z)=(E_1-z)/R_1 \tag{9}$$

where the model parameters involved are, respectively, strength parameter C, effective Rydberg energy R_1 at the Λ point in BZ, CP's energy E_1, discrete excitons energy level $E_{ex,m}$, and broadening constant Γ_1. Again for the $E_1+\Delta_1$ CP, the same expression can be directly employed with $C\rightarrow D$, $E_1\rightarrow E_1+\Delta_1$, and $\Gamma_{1s}\rightarrow\Gamma_1$. Note that the same effective Rydeberg energy is used for both CPs.

Moreover to overcome the long absorption tail resulting from the simple Lorentzian broadening, an energy-dependent broadening expression [22,23] $\Gamma_j'(E)$ have been particularly employed to replace the Lorentzian damping constant Γ_j at E_0, $E_0+\Delta_0$, E_1, and $E_1+\Delta_1$ as

$$\Gamma_j'(E)=\Gamma_j\exp\left[-\beta_j\left(\frac{E-E_j}{\Gamma_j}\right)^2\right] \tag{10}$$

where E_j is the critical point energy, and β_j and Γ_j are the model parameters for the aforementioned CPs. Obviously, when the adjusting parameter β_j is zero, then the Lorentzian broadening can still be hold directly.

To model the contribution of the remaining higher-lying CPs, four damped harmonic oscillators (DHO) [26] have been employed, and the specific form of dielectric function is thus given by

$$\varepsilon^{\mathrm{III}}(E)=\sum_{j=1}^{4}\frac{F_j}{E(j)-E^2-iE\Gamma(j)} \tag{11}$$

where F_j, E_j, and Γ_j are the amplitude, critical point energy, and broadening constant, respectively. Summing the aforementioned contributions together, the total dielectric function thus can be written as

$$\varepsilon(E)=\varepsilon^{\mathrm{I}}(E)+\varepsilon^{\mathrm{II}}(E)+\varepsilon^{\mathrm{III}}(E)+\varepsilon_{\infty} \tag{12}$$

where ε_∞ is an additional real constant to account for the contribution of higher-lying transition out of the investigated region here, and the resulting absorption coefficient can further determined as

$$\alpha(E)=\frac{4\pi}{\lambda}\left(\frac{\left[\varepsilon_1(E)^2+\varepsilon_2(E)^2\right]^{1/2}-\varepsilon_1(E)}{2}\right)^{1/2} \tag{13}$$

with the light wavelength λ in the vacuum. In practice only the contribution coming from the ground state of discrete exciton are considered in our calculation because of the finite effective bound energy. In Table 1, the desirable parameters to model absorption spectrum $\alpha(E)$ of GaSb are shown.

3. Evaluation of thermal radiation dependent performance

On the basis of the calculated absorption coefficient, we mainly in this section concentrate on the structure of absorbing layers and its electric performances relying on the varying incident radiation. The formation of p–n junction cell can be experimentally performed by applying simple zinc-diffused method [27,28] or growing p-type epitaxial layer on the commercially available n-type GaSb substrate. For the present investigation we only consider the latter case because of the unavailability of a realistic Zn-diffused profile at hand. To focus on the structure of absorbing layer associated with external radiation, we assume a typical device doping profiles with acceptor doping concentration $N_A=10^{18}$ cm^{-3} for the p-type emitter while $N_D=10^{17}$ cm^{-3} for the donor doping concentration in n-type base. Additionally, for simplicity the reflection loss at front surface or spectral modulation by the additional antireflection coating (ARC) is neglected.

Following the classical ideal diodes equation without accounting for the effect of series resistance, the basic J–V characteristic for the considered device can be approximately written as

$$J=J_{SC}-J_0\left[\exp\left(\frac{qV}{k_BT_c}\right)-1\right] \tag{14}$$

with J_{SC}, J_0, J, V, T_c, q, and k_B denoting the short-circuit current density, dark current density, operating current density, operating voltage, cell temperature, elementary charge, and Boltzmann's constant, respectively. The dark current density J_0 can be further determined from the device structure as [29]

$$J_0=\frac{qn_i^2D_h}{N_DL_h}\left\{\frac{\sinh(H/L_h)+(S_BL_h/D_h)\cosh(H/L_h)}{\cosh(H/L_h)+(S_BL_h/D_h)\sinh(H/L_h)}\right\}+\frac{qn_i^2D_e}{N_AL_e}\left\{\frac{\sinh(X/L_e)+(S_FL_e/D_e)\cosh(X/L_e)}{\cosh(X/L_e)+(S_FL_e/D_e)\sinh(X/L_e)}\right\} \tag{15}$$

where $X(H)$ is the length of emitter (base) region, n_i is the intrinsic carrier concentration of host material, $S_F(S_B)$ is the surface

recombination rates at the front (back) surface, $D_e(D_h)$ and $L_e(L_h)$ are, respectively, the minority diffusion coefficient and diffusion length. Applying the Einstein relationship, $D_j(j=e/h$ for the electron/hole minority carrier) can be approximately expressed as a function of the minority carrier mobility μ_j, given by

$$D_j = \frac{k_B T \mu_j}{q} \tag{16}$$

where μ_j, in this study, can be further derived from the empirical Caughey–Thomas model [11,27,30] as

$$\mu_{e/h}(N_{A/D},T_c) = \mu_{\min,e/h} + \frac{\mu_{\max,e/h}(300/T_c)^{\theta_{1,e/h}} - \mu_{\min,e/h}}{1+[N_{A/D}/N_{ref,e/h}(T_c/300)^{\theta_{2,e/h}}]^{\alpha_{e/h}}} \tag{17}$$

In the above equation, $\mu_{\min,e/h}$ and $\mu_{\max,e/h}$ represent the value that mobility reaches for very low and high doping level, $N_{ref,e/h}$ is the doping concentration at which the mobility is decreased to half the value it reaches at low doping at room temperature,$\theta_{1,e/h}$, $\theta_{2,e/h}$, $\alpha_{e/h}$ are, respectively, the suggested fitting parameters [11]. The minority carrier diffusion length L_j can thus be further determined as $L_j = \sqrt{D_j \tau_j}$, where the parameter τ_j is the so-called minority lifetime. Considering the notable Auger recombination effect and Shockley–Read–Hall (SRH) trap-assisted recombination mechanism, the minority carrier lifetime in this study is evaluated as

$$\tau_{e/h}^{-1} = (B_{opt}N_{A/D})^{-1} + \tau_{SRH,e/h}^{-1} + (\Lambda N_{A/D}^2)^{-1} \tag{18}$$

where the first term describes the radiation recombination effect with the irradiation recombination coefficient B_{opt}, the second term denotes the trap-assisted SRH recombination, and the last term just represents the Auger recombination effect with the recombination rate Λ.

To determine the short-circuit current density J_{SC}, the internal quantum efficiency of considered device is firstly determined based on the customary addition of the emitter, base, depletion region contribution as

$$QE(\lambda) = QE_E(\lambda) + QE_B(\lambda) + QE_D(\lambda) \tag{19}$$

where the subscript E, B, and D denote the contribution from the emitter, base, and depletion region, respectively, and the specific expression for each component can be found in other places [29]. Integrating the internal quantum efficiency with the incident spectrum $\Phi(\lambda)$, J_{SC} can thus be calculated as

$$J_{SC} = \int_0^{\lambda_m} q\Phi(\lambda)QE(\lambda)d\lambda \tag{20}$$

where λ is the wavelength of incident photon, $\lambda_m(=1.24/E_g)$ is the cutoff wavelength corresponding to the band edge energy E_g, and photon flux density $\Phi(\lambda)$ can be described by Plank-like blackbody irradiation equation as

$$\Phi(\lambda) = \chi\frac{2\pi c}{\lambda^4}\left[\exp\left(\frac{hc}{\lambda k_B T}\right)-1\right]^{-1} \tag{21}$$

where h is the Plank constant, c is the speed of light, and χ is the emissivity of intermediate emitter with the radiator temperature T. All the value of parameters used for the simulation has been summarized inTable 2.

4. Results and discussion

In this section, we evaluate qualitatively the performance perturbation of GaSb absorbing layers depending on the external radiation. Two possible sources, operating temperature T of intermediate radiator and its emissivity χ, are, respectively, discussed.

In Fig. 2, we have schematically depicted the isoefficiency contour plots as a function of the specific size of emitter and base under the illumination of different blackbody spectrum characterized by the specific T. As expected, the higher T is accomplished, the higher η can be attained. Moreover, with the increasing T, the desirable thickness for both emitter and base has a tendency to diminish to achieve the maximum efficiency η. For example, in order to obtain the maximum conversion efficiency 2.07% (solid circle in Fig. 2(a)) for the blackbody spectrum $T=1200$ K, a reasonable structure should be controlled as 180 and 4700 nm for the emitter and base region, respectively, while for the blackbody spectrum $T=1500$ K the corresponding parameter should be thinned as 100 and 4200 nm to receive efficiency 9.4% (solid circle in Fig. 2(c)). As far as the total thickness of GaSb absorbing layers is concerned, the additional width of space depletion region, 110 nm or so for the considered

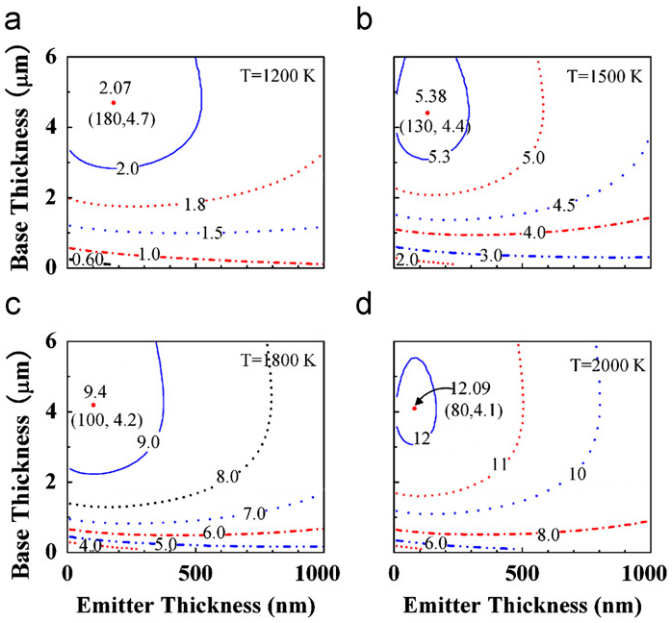

Fig. 2. Isoefficiency contour plot associated with the size of emitter and base under the illumination of different blackbody irradiation characterized by different radiator temperature T.

Table 2
GaSb material parameters for device simulation.

Parameters	Numerical value	Reference	Parameters	Numerical value	Reference
$E_{g,\ 300\,K}$	0.7267 eV	[31]	$\mu_{max,e}$ ($\mu_{max,h}$)	5650 (875) $cm^2\ (V\,S)^{-1}$	
n_i	$1.405\times10^{12}\ cm^{-3}$	[11]	$\mu_{min,e}$ ($\mu_{min,h}$)	1050 (190) $cm^2\ (V\,S)^{-1}$	
B_{opt}	$8.5\times10^{-11}\ cm^{-3}\ s^{-1}$	[10]	$N_{ref,e}$ ($N_{ref,h}$)	$2.8\ (9)\times10^{17}\ cm^{-3}$	[11]
Λ	$5\times10^{-30}\ cm^6\ s^{-1}$	[32]	$\theta_{1,e}$ ($\theta_{1,h}$)	2.0 (1.7)	
$\tau_{SRH,n}$	10 ns	[10]	$\theta_{2,e}$ ($\theta_{2,e}$)	2.8 (2.7)	
$\tau_{SRH,p}$	10 ns	[32,33]	α_e (α_h)	1.05 (0.65)	
S_F	$10^6\ cm\ S^{-1}$	[32,33]	S_B	$10^2\ cm\ S^{-1}$	This work

doping profile, must be included. Phenomenally, with the elevation of T, there is a remarkable improvement of the amount of short-wavelength photon with its energy beyond the fundamental gap, and more and more photon can thus be involved into the generation of electricity, leading to the higher conversion efficiency. In addition, absorption for the short-wavelength photon is generally strong, it is thus very necessary to reduce the thickness of emitter to facilitate the collection of photon-generated minority carrier. Similarly, the same reason can be attributed to the reduction of base thickness. Although any departure from its optimum structure parameters would result in the expected reduction of conversion efficiency, for the real device fabrication, it is still tolerant to obtain an impressive efficiency by relaxing this stringent confinement imposed by the achievement of maximum efficiency to a more extended range, e.g., 100–300 and 3000–5000 nm for the emitter and base, respectively. Note that the size range of this structure relaxation would be shrank with the increment of radiator temperature T, where a larger reduction of conversion efficiency might be encountered. In reality, the suggested structure parameters have been incorporated into the practical process to fabricate GaSb TPV device [2,4].

To see more clearly T-dependent device performance, i.e., the short-circuit current density J_{SC}, open-circuit voltage V_{OC}, fill factor (FF), etc., we have plotted the response of these parameters versus the variation of T in Fig. 3(a) and (b), where the structure parameters of absorbing layers are taken from the optimum one for $T=1500$ K as 130 and 4400 nm for the emitter and base, respectively. As can be seen from Fig. 3(a), all concerned parameters shows evident increase with the upgrading T. Concretely speaking, V_{OC} can be enhanced from 0.39 V for T=1200 K up to 0.48 V for $T=2000$ K, showing 23% improvement only, whereas for J_{SC} this enhancement can be expected from 0.96 up to 32 A/cm^2, showing 31-fold strong improvement, and an analogous behavior can be clarified for the parameters to describe the maximum power point (J_m, V_m). However, due to its current-dominant feature, there is much more apparent discrepancy between V_m and V_{OC} in comparison to the difference between J_{SC} and J_m. Physically, value of the current-associated parameters mainly depends on the amount of photon involved into energy conversion, whereas for the voltage-related performance splitting of quasi-Fermi energy between the p- and n-type region is critical. Consequently, accompanying with the increment of T, great improvement of the number of involved photon gives an astonished increase for the current, and small improvement of voltage output can be attributed to tiny increment of quasi-Fermi energy splitting because of high density of state at the fundamental gap.

In Fig. 3(b), response of η and FF to the variation of T-dependent spectrum is shown. Different from the encouraging enhancement of FF with a positive bowing, the attainable η is very discouraging, only no more than 1% for $T=1000$ K, even the higher temperature 2000 K is realized, the expected efficiency can only reach 13.6%. To circumvent this low efficiency bottleneck, incorporation of an additional selective filter or back reflector has been proposed [1,8], and, for the comparison, this enhanced efficiency η_R by applying spectral filter has also been calculated by means of neglecting the contribution of sub-bandgap to the total incident power density. Apparently, large enhancement of discouraging efficiency encountered in customary configuration can be promised. For example, for the available radiator temperature 1500 K, η can be enhanced from 5.2% for the general configuration up to 25.3% (η_R) for the revised one containing the additional reflector. Additionally, it should be noted that, unlike the nominally visible improvement of conversion efficiency with the help of back reflector, no improvement for the device output

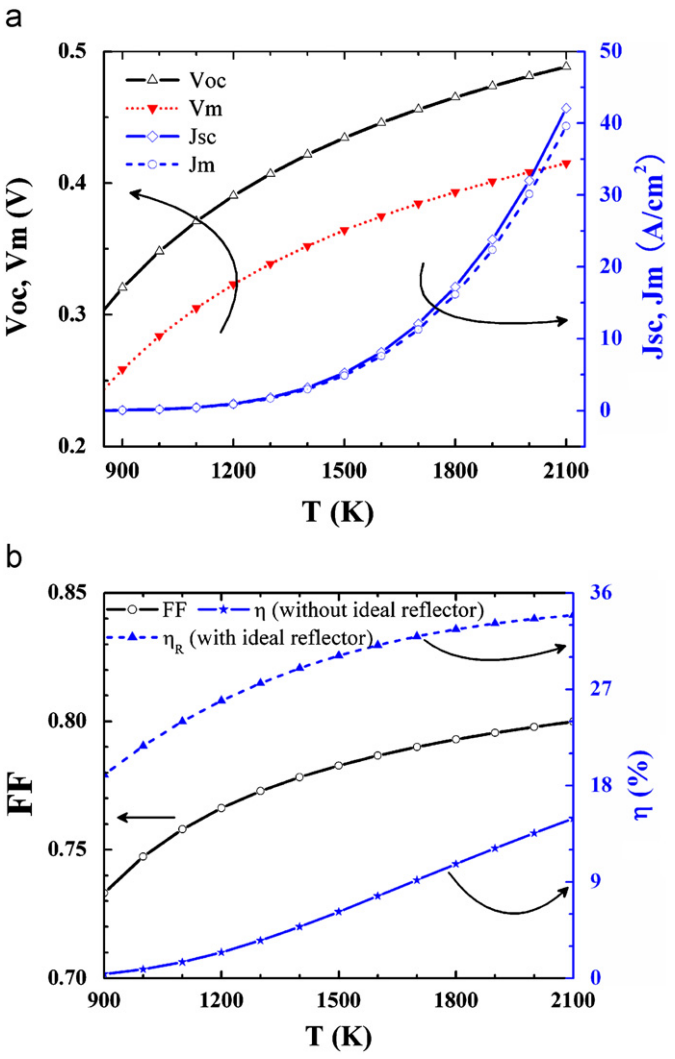

Fig. 3. Response of photoelectric conversion performance to the variation of radiator temperature T: (a) short-circuit current density J_{SC}, open-circuit voltage V_{OC}, and parameters relating to the maximum power point (current density J_m and voltage V_m) are shown. In (b) other concerned parameters, fill factor (FF), customary conversion efficiency (η) and enhanced efficiency (η_R) benefiting from the incorporation of back reflector, are depicted.

such as V_{OC} and J_{SC} can be expected once we neglect the effect of sub-bandgap photon to promote the operating temperature of intermediate radiator. Moreover, the incorporation of back reflector into TPV prototype can effectively change the feature of T-dependent efficiency from a negative bowing into a positive one, implying the enhanced thermal stability of η.

All simulations presented above are based on the assumption of ideal blackbody spectrum, which is far beyond the real situation. For instance, the average emissivity of refractory metal tungsten, a promised candidate for the TPV radiator application, is only no more than 0.5, and this emissivity might also be temperature dependent [34]. Thus it is interesting to evaluate this average emissivity-dependent effect on the practical device performance. In Fig. 4, all concerned characteristic parameters have been schematically depicted as a function of χ, where optimal structure for 1500 K is still assumed. It is easily seen that both V_{OC} and FF show tiny increment with the upgrading χ, whereas the remaining parameters displays strong improvement. Again significant improvement of conversion efficiency is observed by adding the additional back reflector. For instance,

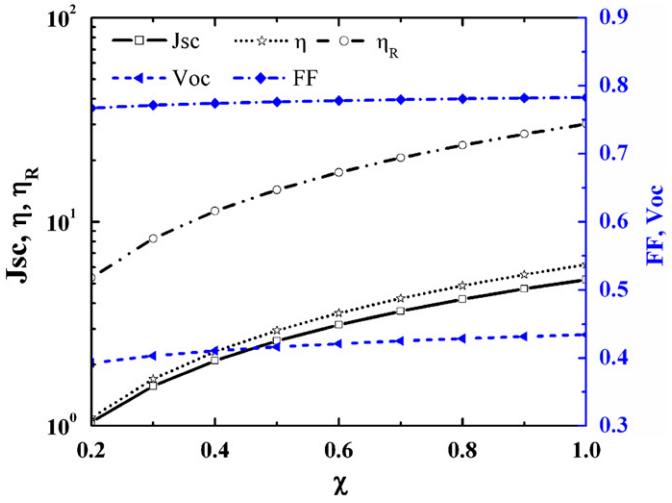

Fig. 4. Emissivity (χ)-dependent device performance.

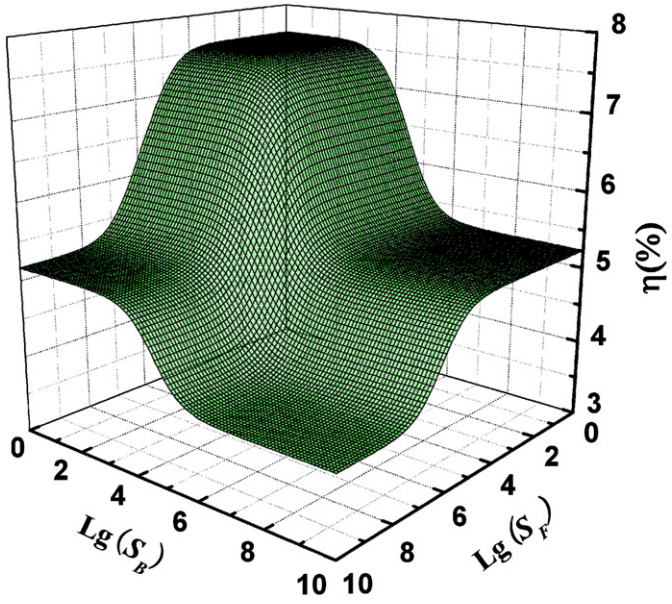

Fig. 5. Effect of surface recombination rates on the conversion efficiency.

the attainable efficiency for the emissivity 0.4, a typical average value for the tungsten, is only 2.4%. If the additional reflector is implemented, the corresponding value for the revised setup can be up to 11.3%, showing fourfold strong improvement. Actually, emissivity of intermediate radiator is a function of the frequency of radiation, thus it is very important to enhance the thermal-to-electric efficiency by artificial engineering to design feasible microstructure [35] to modulate the frequency-dependent emissivity at the interested regions.

Due to the absence of explicit data for the GaSb materials and its device, the back surface recombination S_B was fixed in this study at 10^2 cm/s while the corresponding value for the front surface follows the previous suggestions [32,33]. To reveal the potential effect brought by this unknown parameter, as an illustrative example, we have plotted conversion efficiency versus the variation of S_B and S_F in Fig. 5, where blackbody spectrum $T=1500$ K and its optimal structure parameters are assumed. Evidently, for both surface recombination, the concerned conversion efficiency is invariant when the value of recombination rate located out the sensitive region, 10^3–10^6 cm/s for S_B while 10^4–10^8 cm/s for S_F. Actually, the similar behavior for other parameters such as J_{SC} and V_{OC} is also observed in our simulation for other temperatures. Noticeably, low surface recombination rate is preferential in order to achieve the higher conversion efficiency, indicating the importance of good contact quality in the practical device application, and because of its simple profile qualitative picture discussed above is thus less influenced by this unknown parameter.

5. Conclusion

To sum up, we have improved physical model to express analytically absorption spectrum of GaSb at room temperature in terms of various band critical points of its electronic energy band structure. Our calculated absorption coefficient shows good agreement with the reported experimental data measured by spectral ellipsometry on nominally undoped GaSb sample. Based on this calculated absorption coefficient, we have made an attempt to evaluate qualitatively the structure as well as photoelectric conversion properties of GaSb absorbing layers to the variation of external thermal radiation. Our calculation has demonstrated that optimum thickness to achieve the maximum conversion efficiency should be diminished with the improvement of the amount of photon with energy beyond the fundamental gap. Moreover, performance degradation arising from any size deviation from its optimal one becomes stronger with the increase of radiator temperature. In addition, once the reliable temperature-dependent energy shift and broadening factor of considered critical points is known, then detailed investigations to reveal temperature-dependent performance of GaSb thermophotovoltaic device is promised.

Acknowledgement

This work was supported by the National Basic Research Program of China (973 Program) under Grant no. 2010CB933800.

References

[1] T.J. Coutts, A review of progress in thermophotovoltaic generation of electricity, Renewable Sustainable Energy Rev. 3 (1999) 77–184.
[2] M.G. Mauk, V.M. Andreev, GaSb-related materials for TPV cells, Semicond. Sci. Technol. 18 (2003) S191–S201.
[3] C.A. Wang, Antimony-based III–V thermophotovolatic materials and devices, in: AIP Conference Proceedings, 738, 2004, pp. 255–266.
[4] C.A. Wang, Progress and continuing challenges in GaSb-based III–V alloys and heterostrucutre grown by organometallic vapor-phase epitaxy, J. Cryst. Growth 272 (2004) 664–681.
[5] A.W. Bett, O.V. Sulima, GaSb photovoltaic cells for application in TPV generator, Semicond. Sci. Technol. 18 (2003) S184–S190.
[6] V.M. Andreev, A.S. Vlasov, V.P. Khvostikov, O.A. Khvostikova, P.Y. Gazaryan, S.V. Sorokina, N.A. Sadchikov, Solar thermophotovoltaic convertors based on tungsten emitters, J. Sol. Energy Eng. – Trans. ASME 129 (2007) 298–303.
[7] A. Licciulli, D. Diso, G. Torsello, S. Tundo1, A. Maffezzoli1, M. Lomascolo, M. Mazzer, The challenge of high-performance selective emitters for thermophotovoltaic applications, Semicond. Sci. Technol. 18 (2003) S174–S183.
[8] S. Basu, Y.B. Chen, Z.M. Zhang, Microscale radiation in thermophotovoltaic devices—a review, Int. J. Energy Res. 31 (2007) 689–716.
[9] V.L. Teofilo, P. Choong, J. Chang, Y.L. Tseng, S. Ermer, Thermophotovoltaic energy conversion for space, J. Phys. Chem. C 112 (2008) 7841–7845.
[10] G. Stollwerck, O.V. Sulima, A.W. Bett, Characterization and simulation of GaSb device-related properties, IEEE Trans. Electron. Devices 47 (2000) 448–457.
[11] D. Martín, C. Algora, Temperature-dependent GaSb material parameters for reliable thermophotovoltaic cell modeling, Semicond. Sci. Technol. 19 (2004) 1040–1052.
[12] R. Ferrini, M. Patrini, S. Franchi, Optical function from 0.02 to 6 eV of $Al_xGa_{1-x}Sb$/GaSb epitaxial layers, J. Appl. Phys. 84 (1998) 4517–4524.
[13] D.E. Aspnes, A.A. Studna, Dielectric function and optical parameters of Si, Ge, GaP, GaAs, GaSb, InP, InAs, and InSb from 1.5 to 6.0 eV, Phys. Rev. B 27 (1983) 985–1009.

[14] S. Adachi, Optical dispersion relations for GaP, GaAs, GaSb,InP, InAs, InSb, $Al_xGa_{1-x}As$, and $In_{1-x}Ga_xAs_yP_{1-y}$, J. Appl. Phys. 66 (1989) 6030–6040.
[15] S. Adachi, Optical dispersion relations for AlSb from $E=0$ to 6.0 eV, J. Appl. Phys. 67 (1990) 6427–6431.
[16] A.B. Djurišić, E.H. Li, D. Rakić, M.L. Majewski, Modeling the optical properties of AlSb, GaSb, and InSb, Appl. Phys. A 70 (2000) 29–32.
[17] J.A. Gonzalez-Cuevas, T.F. Refaat, M.N. Abedin, H.E. Elsayed-Ali, Calculation of the temperature and alloy composition effects on the optical properties of $Al_xGa_{1-x}As_ySb_{1-y}$ and $Ga_xIn_{1-x}As_ySb_{1-y}$ in the spectral range 0.5–6 eV, J. Appl. Phys. 102 (2007) 014504.
[18] M. Muñoz, K. Wei, F.H. Pollak, J.L. Freeouf, G.W. Charache, Spectral ellipsometry of GaSb: experiment and modeling, Phys. Rev. B 60 (1999) 8105–8110.
[19] A.B. Djurišić, Y. Chan, E.H. Li, The model dielectric function: application to GaSb and InP, Semicond. Sci. Technol. 16 (2001) 902–908.
[20] M.L. Cohen, J.R. CHelikowsky, in: Electronic Structure and Optical Properties of SemiconductorsSpringer, Berlin, 1989.
[21] A.D. Rakić, M.L. Majewski, Modeling the optical dielectric function of GaAs and AlAs: extension of Adachi's model, J. Appl. Phys. 80 (1996) 5909–5914.
[22] C.C. Kim, J.M. Garland, P.M. Raccah, Modeling the optical dielectric function of semiconductors: extension of the critical point parabolic-band approximation, Phys. Rev. B 45 (1992) 11749–11767.
[23] C.C. Kim, J.M. Garland, H. Abad, P.M. Raccah, Modeling the optical dielectric function of the alloy system $Al_xGa_{1-x}As$, Phys. Rev. B 47 (1993) 1876–1888.
[24] T. Holden, P. Ram, F.H. Pollak, J.L. Freeouf, B.X. Yang, M.C. Tamargo, Spectral ellipsometry investigation of $Zn_{0.53}Cd_{0.47}Se$ lattice matched to InP, Phys. Rev. B 56 (1997) 4037–4046.
[25] K. Wei, F.H. Pollak, J.L. Freeouf, D. Shvydka, A.D. Compaan, Optical properties of $CdTe_xS_{1-x}$ ($0 \le x \le 1$): experiment and modeling, J. Appl. Phys. 85 (1999) 7418–7425.
[26] M. Erman, J.B. Theeten, P. Chambon, S.M. Kelso, D.E. Aspnes, Optical properties and damage analysis of GaAs single crystals partly amorphized by ion implantation, J. Appl. Phys. 56 (1984) 2664–2671.
[27] O.V. Sulima, A.W. Bett, Fabrication and simulation of GaSb thermophotovoltaic cells, Sol. Energy Mater. Sol. Cells 66 (2001) 533–540.
[28] A.W. Bett, S. Keser, O.V. Sulima, Study of Zn diffusion into GaSb from the vapour and liquid phase, J. Cryst. Growth 181 (1997) 9–16.
[29] S. Sze, in: Physics of Semiconductor Devices, Second Ed., John Wiley & Sons, New York, 1981.
[30] D.M. Caughey, R.E. Thomas, Carrier mobility in Silicon empirically related to doping and field, Proc. IEEE 55 (1967) 2192–2193.
[31] Y. Vul'A, Gallium antimonide, in: M. Levinshtein, S. Rumyantsev, M. Shur (Eds.), Handbook Series on Semiconductor Parameters, first vol, World Scientific, Singapore, 1996, pp. 125–146.
[32] D. Martin, C. Algora, Key Issues for an accurate modeling of GaSb TPV converters, in: AIP Conference Proceedings, 653, 2003, pp. 442–451.
[33] C. Algora, D. Martin, Modelling and manufacturing GaSb TPV converters, in: AIP Conference Proceedings, 653, 2003, pp. 452–461.
[34] R.D. Allen, L.F. Glasier, P.L. Jordan, Spectral emissivity, total emissivity, and thermal conductivity of molybdenum, tantalum, and tungsten above 2300 K, J. Appl. Phys. 31 (1960) 1382–1387.
[35] H. Sai, H. Yugami, Y. Kanamori, K. Hane, Solar selective absorbers based on two-dimensional W surface gratings with submicron periods for high-temperature photo-thermal conversion, Sol. Energy Mater. Sol. Cells 79 (2003) 35–49.